THE JOURNAL OF PHYSICAL CHEMISTRY B

ARTICLE

pubs.acs.org/JPCB

The Phases in a Non-Ionic Surfactant ($C_{12}E_6$)−Water Ternary System: A Coarse-Grained Computer Simulation

N. Denham, M. C. Holmes,* and A. V. Zvelindovsky

Centre for Material Science, University of Central Lancashire, Preston, PR1 2HE, United Kingdom

ABSTRACT: A dissipative particle dynamics computer simulation is used to investigate the ability of small oil molecules (hexane, dodecane, and octadecane) to control phase structures in nonionic surfactant−water systems. The model is successfully tested against the experimental results for binary and ternary systems where the third components are "swelling" and "penetrating" oils. The experimentally observed phases present in such systems were successfully modeled. In addition, the simulations show the locations of the oil molecules within the bilayer and the surfactant chain conformation. While the simulations confirm much of what is expected from experiment and theoretical models, evidence is found for the terminal methyl end of the surfactant molecules being located slightly closer to the interfacial region than other groups in the same chain.

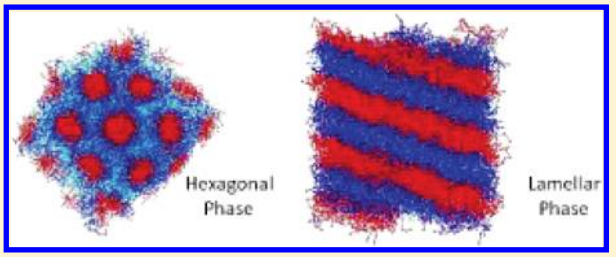

1. INTRODUCTION

Surfactant−water mixtures act as simple models of lipid water systems that form the basis of biological membranes. A key feature of surfactant−water mixtures (including lipids) is the interface between the aqueous and hydrophobic regions. Phase structures are distinguished by the curvature of this interface: as the interface changes curvature, the equilibrium phase structure changes. While this curvature is controlled by the concentration of surfactant and by temperature, it can also be controlled by the addition of molecules. These molecules can be both small and simple, such as oils and alcohols, or they can also be functionally more important, for example, for lipid systems, anesthetics, or small peptides such as antimicrobial peptides. It may be possible that the structural changes that are induced by these molecules can be understood in terms of the changes in interfacial curvature that they promote.

We have studied experimentally the effects of adding small molecules (oils, alcohols, and anesthetics) to simple nonionic surfactant systems ($C_{12}E_6/H_2O$, etc).[1−3] In the case of oils, the changes in curvature are understood in terms of there being two extreme types of behavior,[4] namely, that when the oil chain length is much shorter than the surfactant chain length the oil penetrates between the chains, increasing the headgroup area at the interface, s_a. This may result in the lamellar spacing decreasing slightly or staying constant depending upon surfactant alkyl chain packing.[3] These are described as penetrating oils. In contrast when the oil chain length is longer than that of the surfactant chain the oil does not penetrate, and does not change s_a, but it does swell the hydrophobic region. These are described as swelling oils. Both behaviors have different effects upon the interfacial curvature and upon the phase structure. The addition of other molecules, such as anesthetics which are structurally more complex, results in more complex behavior.

Intermediate mesh phases have been established for some time both in surfactant−water systems[5] and in diblock copolymers.[6] There are several possible phase structures: rhombohedral mesh,[2,3] tetragonal mesh,[7] random mesh,[2,3] and a variety of ribbon phases.[8] They are unique in the pantheon of phase[9,10] structures in that the interfacial curvature between the aqueous and nonaqueous regions is not uniform. They tend to either be metastable or exist in a small region of the phase diagram, although there are exceptions.[11] These structures are of interest for their potential to act as templating media and also model systems to study the changes in interfacial curvature on the addition of small molecules.

Wang[3] investigated the effect of adding oils to the $C_{16}E_6$/water system and found that adding oil to mesh phases destabilized the phase in favor of the lamellar phase. Adding oil at a fixed alkyl chain volume fraction decreases the mean interfacial curvature, resulting in the loss of phases with a high mean curvature. When a sufficient amount of oil is added, even the lamellar phase is destabilized, and the system phase separates. Swelling and penetrating behavior was also observed by Kunieda et al.,[12−14] where decane, *m*-xylene, or squalene was mixed with $C_{12}E_n$, where *n*, the length of the headgroup, was varied. Decane acted as a swelling oil for both $C_{12}E_3$ and $C_{12}E_7$ surfactants, where the transitions $L_\alpha-H_2$ and H_1-I_1 were observed for $C_{12}E_3$ and $C_{12}E_7$, respectively.

In previous experimental studies on the hexaethylene glycol *n*-hexadecyl ether ($C_{16}E_6$)/water system,[9,15] the phase diagram was investigated, and the phase structures identified on heating and cooling. The system shows a rich series of stable and

Received: September 20, 2010
Revised: December 10, 2010
Published: January 25, 2011

metastable phases. At 55% by weight of surfactant, it shows the following sequences:

$$\textit{Cooling}: L_\alpha \rightarrow 45\ ^\circ C \rightarrow \mathrm{Mh}_1(0) \rightarrow 33\ ^\circ C \rightarrow \mathrm{Mh}_1(R\bar{3}m) \rightarrow 29\ ^\circ C \rightarrow V_1(Ia3d) \rightarrow 27\ ^\circ C \rightarrow H_1 + L_\alpha$$

$$\textit{Heating}: H_1 + L_\alpha \rightarrow 27\ ^\circ C \rightarrow V_1(Ia3d) \rightarrow 33\ ^\circ C \rightarrow \mathrm{Mh}_1(0) \rightarrow 45\ ^\circ C \rightarrow L_\alpha$$

where L_α is a classical lamellar phase, $\mathrm{Mh}_1(0)$ is a disrupted lamellar or random mesh phase, $\mathrm{Mh}_1(R\bar{3}m)$ is an intermediate mesh phase, $V_1(Ia3d)$ is a normal bicontinuous cubic phase, and $H_1 + L_\alpha$ is a two-phase hexagonal plus gel phase region, with the nomenclature of the mesh phases adopted from ref 5.

In the experimental work, hexane, decane, and octadecane were added to the nonionic surfactant $C_{16}E_6$, which is similar to the surfactant being modeled, $C_{12}E_6$. The oils are also equivalent except for decane (experiment) and dodecane (simulation), but both are of similar length to the tail of the surfactants to which they are added. Hexene and hexane are equivalent in this case, as the simulation of hexane uses just two beads separated by a single, straight bond.

The aim of these experimental studies has been to understand how the addition of small molecules to surfactant−water systems changes the interfacial curvature and hence the phase structure. Understanding this relationship would not only allow the manipulation of surfactant−water phase structure for such applications as templating new materials but could also lead to a better understanding of the interaction of small molecules, such as anesthetics, and larger peptides with biological membranes. One way to do this more effectively may be through the use of computational models.

The supramolecular structures we study require long equilibration times due to the nature of the formation of these structures. Atomistic molecular dynamics is computationally too costly for such systems, and a coarse grained approach is more appropriate. Dissipative particle dynamics (DPD), which was first introduced by Hoogebrugge and Koelman,[16] can be applied to such surfactant−water systems. This approach has the advantage of producing correct hydrodynamic behavior on large length and time scales and makes it suitable for simulating surfactants in aqueous solution as well as many other complex fluids.[17,18]

In 2001, Groot and Rabone[19] mapped Flory−Huggins parameters for surfactant−water systems and also performed a length scaling. A simple DPD simulation of surfactants in aqueous solution has been using a dimeric model,[20] where the surfactant has been represented by two connected beads; one was the hydrophilic head, and the other, the hydrophobic tail. This reproduces the standard lyotropic phases, such as micellar, hexagonal, and lamellar. In another study,[21] a mesh phase and a bicontinuous phase were observed.

In ref 22, the surfactant $C_{12}E_5$ was modeled using four beads for the tail and six beads for the head (A_4B_6); one for each of the polyoxyethylene groups and a further one for the terminal OH group. Water was represented by one bead. Although the micellar and lamellar phases were obtained using this method, each bead represents an identical volume, so the beads' coarse graining was incorrect for the surfactant molecule. In ref 23, $C_{12}E_6$ was modeled using a dimeric model. Although just two beads were used, the volumes of the tail and head parts for $C_{12}E_6$ are comparable to experiment. It was found that the lamellar, hexagonal, and micellar structures are stabilized depending on the strength of the water−head repulsion parameter. The standard phases were also stable phases in ref 24 using amphiphilic models A_1B_1 and A_1B_3 in two different solvents. Adding oil (decane) to the surfactant $C_{10}E_4$ as a third component to a surfactant−water system was studied in ref 25. The results were obtained only for a very limited range of concentrations, and either macro phase separation or the bicontinuous phase was observed.

DPD has also been used to investigate model lipid bilayers.[26,27] Groot and Rabone[19] also applied the DPD method to biological membranes. In most systems, the bilayer phase occurs when the tails of the surfactants do not interdigitate; however, in some instances, this interdigitation does occur.[28,28]

In this paper, we use a dissipative particle dynamics (DPD) regime to investigate the ability of small molecules to control phase structures in nonionic surfactant−water systems. The model is tested against binary and ternary surfactant−water systems where the third component is an oil. The experimental data that we have for this system provides an excellent check of the model and methodologies.

2. METHOD

The DPD model is proposed with N particles moving in a continuum domain of volume V. These particles or "beads" represent a cluster or group of atoms or molecules. The system is updated in discrete time steps Δt. The time evolution of the particles of mass m_i is governed by Newton's equations of motion which have been set out in detail by Moeendarbary et al.[17] and by Groot and Warren:[29]

$$\frac{\mathrm{d}\mathbf{r}_i}{\mathrm{d}t} = \mathbf{v}_i, \qquad \frac{\mathrm{d}\mathbf{v}_i}{\mathrm{d}t} m_i = \mathbf{F}_i$$

The total force on a given particle i is

$$\mathbf{F}_i = \sum_{j \neq i} \mathbf{F}_{ij}^{\mathrm{C}} + \mathbf{F}_{ij}^{\mathrm{D}} + \mathbf{F}_{ij}^{\mathrm{R}}$$

where $\mathbf{F}_{ij}^{\mathrm{C}}$ is a conservative force, $\mathbf{F}_{ij}^{\mathrm{D}}$ is a dissipative force,and $\mathbf{F}_{ij}^{\mathrm{R}}$ is a random force:[30]

$$\mathbf{F}_{ij}^{\mathrm{D}} = -\gamma \omega_{\mathrm{D}}(r_{ij})(\mathbf{e}_{ij}\mathbf{v}_{ij})\mathbf{e}_{ij}$$

$$\mathbf{F}_{ij}^{\mathrm{R}} = \sigma \omega_{\mathrm{R}}(r_{ij})\mathbf{e}_{ij}\zeta_{ij}$$

$$\mathbf{F}_{ij}^{\mathrm{C}} = \begin{cases} a_{ij}(1 - r_{ij})\hat{\mathbf{r}}_{ij} & (r_{ij} < r_{\mathrm{c}}) \\ 0 & (r_{ij} \geq r_{\mathrm{c}}) \end{cases}$$

where $r_{ij} = |r_i - r_j|$, $e_{ij} = (r_i - r_j)/r_{ij}$, $v_{ij} = v_i - v_j$, and ζ_{ij} is a Gaussian white noise term with $\zeta_{ij} = \zeta_{ji}$ and $\langle \zeta_{ij}(t) \rangle = 0$. Also, a_{ij} is the interaction parameter between particle i and j, and a is a dimensionless parameter which gives the strength for the repulsion between particles i and j. ω_{D} and ω_{R} are weight functions that ensure that $\mathbf{F}^{\mathrm{R}}$ and $\mathbf{F}^{\mathrm{D}}$ vanish when r_{ij} becomes greater than r_{c}, a cut-off distance for the forces.

Parameterization. *Units.* DPD units of length, energy, and time are denoted by σ, ε, and τ, respectively. The unit of length, r, can be based on the cut-off distance r_{c}, so $r_{\mathrm{c}} = 1$. The volumes of the beads are the same, and the masses of the beads are similar. For simplicity, the mass of all of the beads is 1, and the unit of energy is $k_{\mathrm{B}}T = 1$.

Time Step. The unit of time, τ, is set to $r_{\mathrm{c}}(m/k_{\mathrm{B}}T)^{1/2}$. The time step Δt is chosen as 0.06. An additional constant λ associated

Table 1. Densities and Volumes for Water, Hydrocarbon, and Oxyethylene Groups

	density (kg m^{-3})	volume (nm^3)
H_2O	1000	0.030
$CH_3(CH_2)_{11}$	750[33]	0.380
$(OCH_2CH_2)_6OH$	1123[34]	0.420

with the time integration due to the stochastic interactions is set to 0.65. Using $\lambda = 0.65$, the time step for a simulation at $k_BT = 1$ can be up to 0.06 with only a temperature rise of 1%.[31] The noise term σ was chosen to ensure relatively fast temperature responses while reducing the inherent temperature increases. With $k_BT = 1$, this means that $\gamma = 6.75$.

The Repulsion Parameter. As the DPD technique is based on soft sphere interactions, the repulsion parameter a needs to be chosen while taking into account the compressibility of the system. We used the method of Groot and Warren[29] who simulated water using DPD beads and measured how the pressure of the system varied as a function of the bead density. Taking the compressibility of water, 4.5×10^{-10} m^2 N^{-1}, and the number density of water molecules 3.35×10^{28} m^{-3}, we obtain

$$a = 75k_BT/\rho$$

As ρ should be as low as possible to minimize the computational time, we took $\rho = 3$. This means that for $k_BT = 1$ the repulsion parameter for like beads is 25 for water.

Hydrophobic Repulsion. To model the hydrophobic effect, an excess repulsion is added for the interactions between water and tail beads and head and tail beads. The excess or hydrophobic repulsion parameter is denoted by Δa. Since the simulation system is quite incompressible, this model should be quite close to the Flory−Huggins lattice model. Groot and Warren[32] mapped the Flory−Huggins model onto Δa using the free energy per lattice site F. Groot and Rabone[31] used a water−hydrocarbon Flory−Huggins parameter of 6 and found that three water molecules are represented by one bead, and this is largely independent of temperature. Using this value gives $\Delta a = 21$. We have used this as a rough guide for preliminary simulations, but different Δa values will be investigated to find the optimum value that matches experimental behavior.

Length Scale. A DPD bead volume needs to be chosen so that each bead is an effective represention of water, hydrocarbons, and oxyethylene. Table 1 shows the density and volume for H_2O, $CH_3(CH_2)_{11}$, and $(OCH_2CH_2)_6OH$.

By choosing the DPD bead volume as 0.09 nm^3, each DPD bead represents the volume of three water molecules, the volume of a $(CH_2)_3$ group, and the volume of 1.5 CH_2CH_2O groups. The nonionic surfactant $C_{12}E_6$ can therefore be conveniently modeled using four tail beads and four head beads connected in a single chain with harmonic bonds. The molecule is therefore being represented by a coarse grained model A_4B_4, where A and B represent head and tail beads, respectively. A water bead represents three water molecules. Groot and Warren[32] have shown that the volume of each bead is $V_B = 0.09$ nm^3 and, with $\rho = 3$, r_c has the value 0.64633 nm.

Bonds. The beads in the surfactant are connected with bonds modeled using harmonic springs:

$$U_{bond}(r) = \frac{1}{2}k(r - r_0)^2$$

Table 2. Parameters and Values Selected for the Model

parameter	value
time step (Δt)	0.06τ
cut-off distance (R_c)	0.65 nm
reduced energy scale (k_BT)	1
repulsion parameter for like beads (a_{BB})	25
number density of beads (ρ)	3
volume per bead	0.09 nm^3
length of bond	0.65 nm
spring constant for harmonic bonds (k)	$100\varepsilon\sigma^{-2}$
excess repulsion for unlike beads (Δa)	15
box side length	14.5 nm

where r_0 is the equilibrium bond length and k is the spring constant. The all-*trans* length of $C_{12}E_6$ is 3.57 nm. Dividing this value by (number of beads − 1) representing the number of bonds (7) gives 0.51 nm ∼ r_c. The optimum bond strength k might be obtained from the vibrational frequencies of carbon−carbon bonds from infrared spectroscopy; however, for a coarse grained model, each DPD bond consists of several bonds coupled together, making this method difficult.

An appropriate way to determine k is to find the lowest value that corresponds to an equilibrium bond length of $r_c = 0.646$ nm, with a standard deviation of 1%. A simulation of 3051 A_4B_4 molecules was arbitrarily introduced into a simulation cube of side 14.5 nm. All of the parameters were as chosen in Table 2, where $\Delta a = 15$. Three different k values were chosen, 10, 100, and $200\varepsilon\sigma^{-2}$. The mean and standard deviation bond lengths were measured from 50 bonds. For $k = 100\varepsilon\sigma^{-2}$, the equilibrium bond length is within 1% of r_c. The standard deviation also decreases significantly from $k = 10\varepsilon\sigma^{-2}$ to $k = 100\varepsilon\sigma^{-2}$. The mean and error in bond lengths do not change significantly for spring constant values higher than $100\varepsilon\sigma^{-2}$; therefore, $k = 100\varepsilon\sigma^{-2}$ was chosen.

3. RESULTS AND DISCUSSION

Binary System. *Determining the Excess Repulsion Parameter, Δa.* The $C_{12}E_6$ water system was investigated by Clunie et al.[35] and its phase diagram established. This shows that the most dominant phases are L_1, H_1, and L_α, with a small region of V_1 lying in between the H_1 and L_α phases. At room temperature, the phase sequence upon increasing concentration is

$$L_1 \xrightarrow{40\%} H_1 \xrightarrow{65\%} V_1 \xrightarrow{70\%} L_\alpha$$

A series of simulations was performed at different concentrations to reproduce the phase sequence, starting with an excess repulsion parameter of $\Delta a = 21$.[32] The numbers of waters and surfactants for each concentration were calculated using the molecular weight of $C_{12}E_6$ and water molecules so that each concentration can be represented by an equivalent percentage by weight $C_{12}E_6$. A simulation box of side 14.5 nm was chosen, giving potentially six lamellar repeats from corner to corner at a surfactant concentration of 100%. Simulations were for at least 100 000 time steps, although further steps were undertaken if necessary until equilibrium was established, judged from the stabilization of the total energy of the system.

After each simulation, the structures were identified by visual inspection of the simulation. The results of these simulations from 50 to 95% by weight concentrations of surfactant in 5% graduations

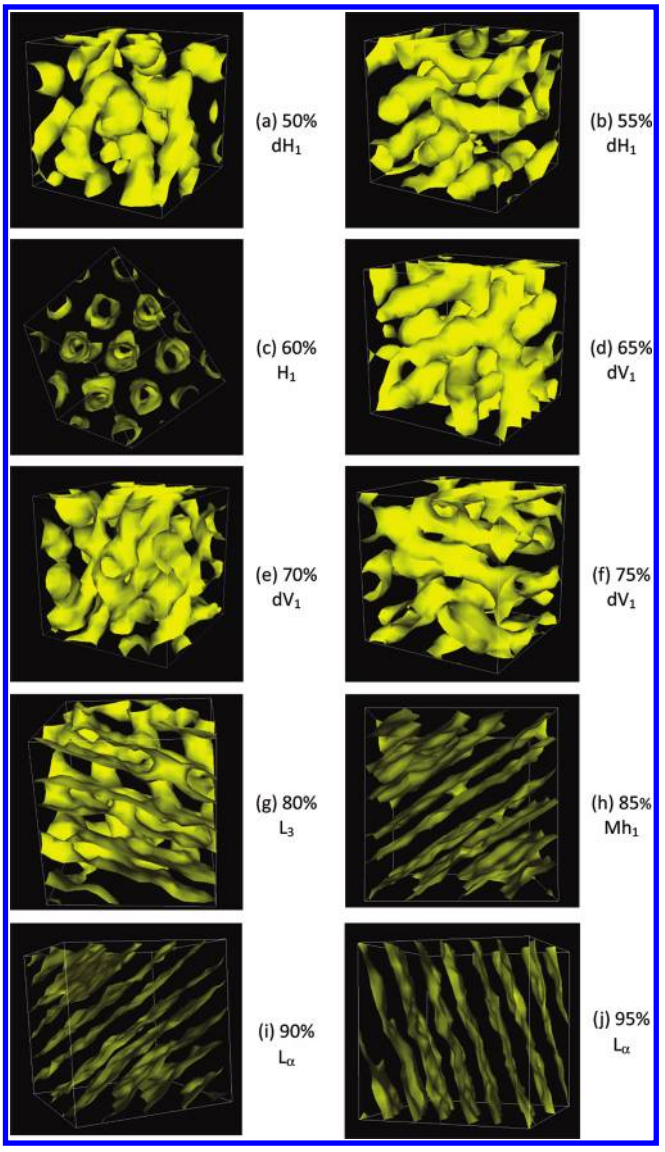

Figure 1. Isodensity surface images of $C_{12}E_6$/water simulations after 100 000 time steps, showing the interface between the head and the tail region. The phase nomenclature is standard,[5] but where a phase is significantly disordered this is indicated by the prefix"d".

are shown as iso-density surfaces (showing the interface region) in Figure 1.

Figure 2 shows a ball-and-stick model of the surfactants with the water beads. From these figures, it can be seen that the water beads pack within the headgroup region.

At 50 and 55%, there is aggregation of the surfactants into elongated micelles, and the phase is considered to be a cylindrical type phase. However, as the cylinders have no particular orientation with respect to each other or show any interaggregate order, this phase will be referred to as a disordered hexagonal phase (dH_1). Increasing the concentration to 60%, the cylinders elongate, forming apparently "infinite" cylinders which are hexagonally packed, i.e., hexagonal phase (H_1). Increasing the concentration to 65%, the structure changes to interconnected cylinders arranged in an irregular fashion. The interconnections are largely 3-fold, as are many real bicontinuous structures. However, this phase does not show any regular order and will be referred to as a disordered bicontinuous phase (dV_1). At 80%, some layer-like patterns appear.

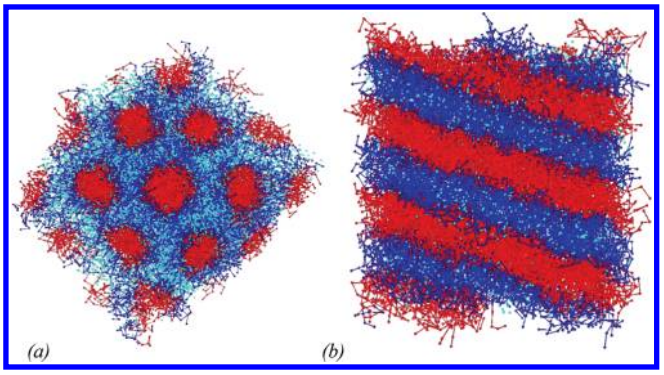

Figure 2. Bead-stick images of (a) the H_1 phase (60%) and (b) the L_α phase (90%). Dark blue represents head beads, light blue represents water beads, and red represents tail beads.

However, this phase is also disordered, with pores and interconnections between the layers resembling the sponge phase (L_3) studied experimentally.[36,37] At 85%, there are layers that have water filled defects or pores, and this phase will be referred to as the mesh phase (Mh_1). From 90 to 100%, the phase is lamellar (L_α).

The excess repulsion parameter, Δa, was then tuned to produce the best match between the simulated and experimental phase behavior. For a simulation cube of side 14.5 nm, concentrations between 50 and 100% by weight $C_{12}E_6$ were simulated for Δa = 10, 15, and 20 (a_{ij} = 35, 40, and 45, respectively). Simulations were performed until equilibrium was attained.

The lamellar phase is most stable for $\Delta a = 15 \pm 5$. For $\Delta a = 10$, the excess repulsion is too low, so there is insufficient hydrophobic force for the lamellar phase to form until high concentrations. For $\Delta a = 20$, the excess repulsion seems to be too strong, and a sponge-like phase L_3 becomes stable where a lamellar phase should be found if the parameters were relaxed enough to allow it to form. The excess repulsion was chosen to be $\Delta a = 15$ ($a_{ij} = 40$).

Determining the Head-to-Head Interactions, a_{BB}. Polyoxyethylene chains readily form hydrogen bonds with water molecules,[38] so that it is more energetically favorable for water molecules to mix in between oxyethylene molecules in a polyoxyethylene−water mixture. This implies that the interaction parameter between head groups should be higher. A set of simulations were performed with varying concentrations using $\Delta a = 15$, changing a_{BB}, the repulsion parameter for head-to-head interactions from 25 to 35 (close to the hydrophobic repulsion parameter). The results of these simulations are shown in Figure 3.

As the headgroup-to-headgroup interaction parameter is increased, phases with layer-like structure (sponge, mesh, and lamellar) are destabilized in favor of phases that have positive surface curvature (e.g., bicontinuous). For example, with a_{BB} = 25, the lamellar phase is present at 90%, but on increasing a_{BB} to 30, the lamellar phase is still not stable at 95%. It seems apparent that, at these higher concentrations, where there are fewer water beads, there is a stronger repulsion between the head groups than the tail groups, which discourages the formation of layer-like phases. As in experimental systems, the lamellar phase is quite stable, even at lower concentrations. It is appropriate to choose a_{BB} where these layer-like phases are most stable, so $a_{BB} = 25$ was chosen.

Finite Box Size Effect. As the number of particles modeled is small compared to a real system, apparent large scale behavior may be caused by introducing the periodic boundary conditions

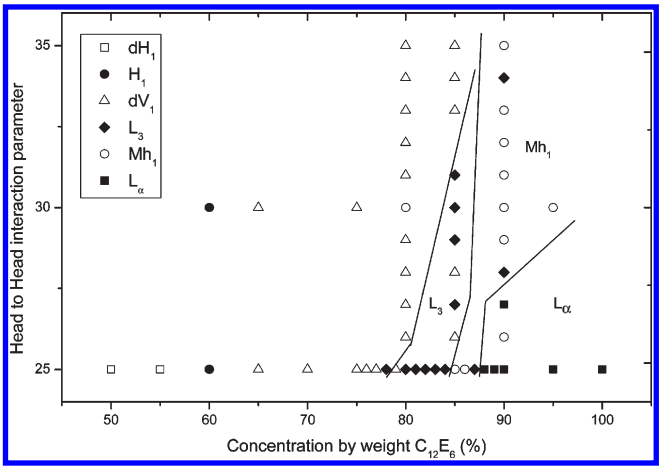

Figure 3. Phase diagram showing phase sequences for different head-to-head interaction parameters. Lines are a guide to the eye.

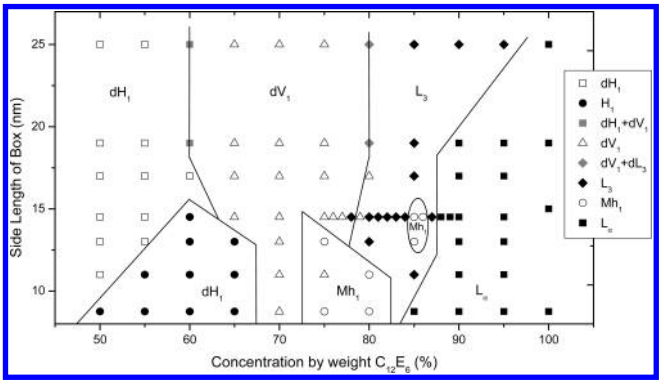

Figure 4. Phase diagram showing the phase sequence for different box sizes. Lines are a guide to the eye.

associated with a finite box size. A set of simulations was performed for concentrations from 50 to 100%, varying the size from 8.75 to 25 nm. Simulations were performed for at least 100 000 time steps, or until total energy equilibrium was achieved. Figure 4 shows the results from this set of simulations.

Starting from the smallest box size (8.75 nm), the phase sequence is clear, and the structures show a high degree of inter-aggregate order. The phase sequence is

$$H_1 \xrightarrow{67.5\%} dV_1 \xrightarrow{72.5\%} Mh_1 \xrightarrow{82.5\%} L_\alpha$$

However, as the box size increases, the stability of these ordered phases decreases. The mesh phase region is not stable at box sizes larger than 11 nm, and the hexagonal phase is not stable at box sizes larger than 13 nm. In place of the H_1 phase, a dH_1 phase becomes dominant, and in place of the Mh_1 phase, the L_3 phase becomes dominant. Also, the dV_1 phase becomes dominant over a larger concentration range. At 13 and 14.5 nm, there is a small region of a mesh phase between L_α and L_3. This phase has fewer pores than the main mesh phase region, and is more like a random mesh phase ($Mh_1(0)$).

From this phase diagram, it can be seen that while the sequence of phases remains unchanged the range and stability of the phases is affected. The changes seem to be reduced as the box size increases above 17 nm, above which the phase sequence remains fairly constant; however, this is after the majority of the ordered phases have been lost. The question that needs to be asked here is whether the smaller box size induces the ordered phases or whether the larger box size destabilizes the ordered phases.

Simulation box sizes are generally considered in relation to the cut-off distance for interactions. If the box size is of the same order as the cut-off distance, then one bead may have an interaction with itself, due to periodic boundary conditions. As an absolute minimum, a box size of at least twice the cut-off distance is normally chosen. The cut-off distance for these simulations is 0.65 nm, and the smallest box size is 8.75 nm. The repeat distance for the lamellar phase in these simulations is approximately 4 nm, so the box size should be at least 8 nm. One final consideration is that the boundary conditions limit the number of possible orientations of the phases, effectively quantizing the values for the repeat distances. The smaller the box size is, the larger the quantization effect.

In order to choose an appropriate box size, a compromise must be made between a large box where ordered phases are less stable and a small box where there are too few repeat distances of phases inside the simulation cell. 14.5 nm has been chosen here, as the H_1 phase is still stable and Mh_1 phases are stable, but there is still enough for approximately 5−6 repeat distances of the lamellar phase.

The parameters set for these simulations have been determined either from theory or by comparison with experiment and are summarized in Table 2.

Oil Addition. *Modeling Oil.* Oils possess the same properties as the surfactant alkyl chains and are therefore modeled representing a chain of three hydrocarbons by one DPD bead and using the same repulsion parameters, bond length, strength, etc. The three oils were hexane (two beads), octadecane (six beads), and one that has the same length as the surfactant tail dodecane (four beads). The results are compared with the experimental addition of hexane (penetrating), decane, and octadecane (swelling).[4]

The oils were added to surfactant−water mixtures with surfactant-to-water mole ratios of 0.12, 0.16, 0.23, 0.36, and 0.75. This corresponded to the binary surfactant concentration by a weight range of 75−95%, which exhibits the phase sequence:

$$dV_1 \xrightarrow{77.5\%} L_3 \xrightarrow{82.5\%} Mh_1 \xrightarrow{87.5\%} L_\alpha$$

The number of surfactant molecules, oil molecules, and water beads in each simulation was calculated from the molecular weights of each of the molecules and the mole ratio of surfactant to water and the mole fraction of oil.

The phase diagrams showing the phases from the addition of different mole fractions of hexane, dodecane, and octadecane to different surfactant-to-water mole ratios are shown in Figure 5.

Experimentally,[3] all of the oils destabilize phases with more surface curvature in favor of those phases with less or no surface curvature; while this is confirmed by the simulations with hexane and dodecane, that with octadecane is different. It shows an extensive disordered bicontinuous phase extending to high oil concentrations. Experimentally, the longer the molecule introduced, the lower the stability of phases with curvature.

Comparing the phase boundaries for hexane (Figure 5a) with those for dodecane (Figure 5b) shows that the phases are destabilized at lower mole fraction of oil for dodecane than that for hexane which is consistent with the experiment. Larger molecules have a larger volume, and will give a larger contribution to the alkyl chain volume fraction of the phase, encouraging phases with lower surface curvature to form. Figure 6 shows the phase diagrams drawn using oil volume fraction.

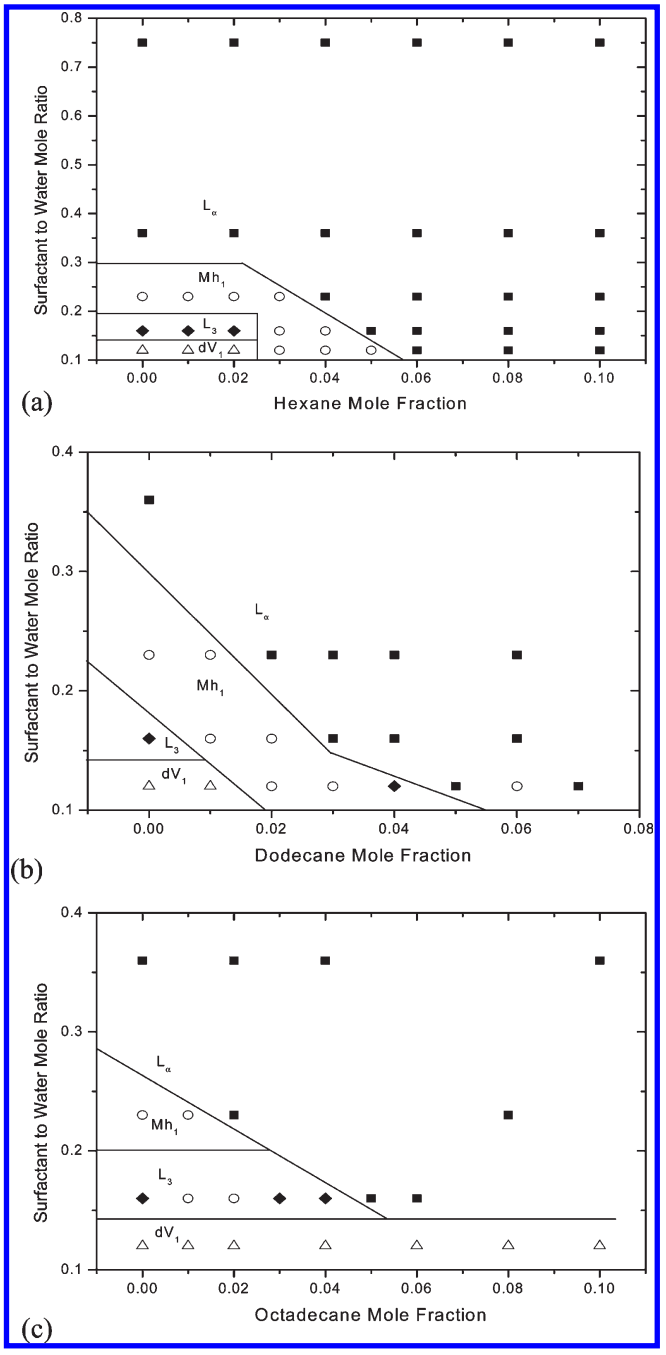

Figure 5. Simulated phase diagrams: surfactant−water ratio versus mole fraction of oil in a 14.5 nm box. The phases are L_α (■), Mh_1 (○), L_3 (◆), and dV_1 (△). Lines are a guide to the eye.

The addition of both hexane and dodecane give similar phase boundaries. However, for octadecane, all phase transitions are at considerably higher oil volume fractions. Therefore, it is unlikely that a simple volume effect is the only process at work here.

Oil Behavior in the Tail Region. From experiment, octadecane should behave like a swelling oil, whereas hexane should behave as a penetrating oil. The swelling and penetrating behavior can be observed by measuring the repeat distance, d_0, of the lamellar phase as a function of the mole fraction of added oil. It should be noted that the finite size of the cell used for the simulations causes d_0 to be quantized and therefore the changes appear to be "stepped". d_0 has been calculated for the addition of

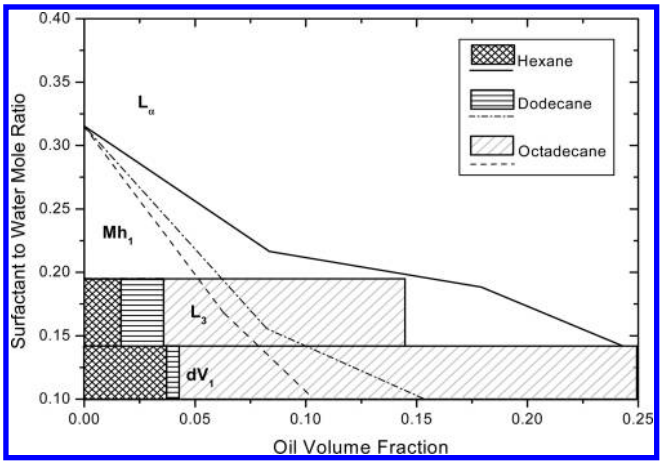

Figure 6. Composite phase diagram for all three oils as a function of oil volume fraction.

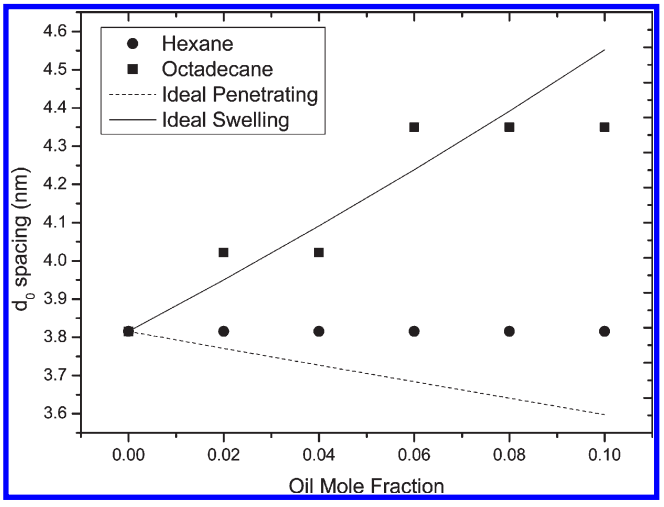

Figure 7. Ideal penetrating and swelling behavior for hexane and octadecane, respectively, compared to simulation results. The ideal penetrating and swelling curves were calculated from eqs 2 and 3 of Wang et al.[3]

hexane, dodecane, and octadecane in simulations at X_{sw} = 0.75 and oil mole fractions from 0.02 to 0.10 in 0.02 steps. The results of these are shown in Figure 7. The addition of hexane has no effect on the bilayer spacing within the limits of the quantization effect, its behavior being between ideal swelling and penetrating oils. Octadecane shows the most swelling behavior from 3.8 nm to about 4.3 nm at 0.06 mol fraction of oil and behaves very much like an ideal swelling oil. Dodecane produces a modest increase in d_0 from 3.8 to 4.0 nm (not plotted in Figure 7 for clarity), demonstrating some swelling of the bilayer.

The close similarity between computational results, experiment, and theory lends confidence to the DPD method used.

Bilayer Composition. Using the DPD model, the location of the oil molecules in the hydrophobic region can be explored by evaluating the probability density functions of the beads representing the different moieties within the lamellar phase for each oil. A surfactant−water mole ratio of X_{sw} = 0.75 was used because it gave lamellar structures. Bead probability density function plots were created by taking the coordinates of every bead from the output file of the DPD simulation across the lamellar bilayer for the tail, head, oil, and water beads. Figure 8 shows an example of

the bead probability density functions produced for all types of beads across a single lamellar layer.

This can be repeated for the series of four oils at a range of oil concentrations. As the concentration of oil increases, the oil peak also grows, while the tail peak becomes lower and broader. The tail peak also flattens at large concentrations, and in the cases of dodecane and octadecane, the tail peak starts to separate into two peaks. The behavior is demonstrated by the extremes of hexane and octadecane shown in Figure 9.

This behavior is summarized in Figure 10 where the peak full widths at half-maximum (fwhm) are plotted as functions of oil mole fraction. The fwhm's for the distribution of the oil beads were obtained by fitting the curve to a single Gaussian curve, while those for the tail beads were obtained by fitting to two Gaussian curves.

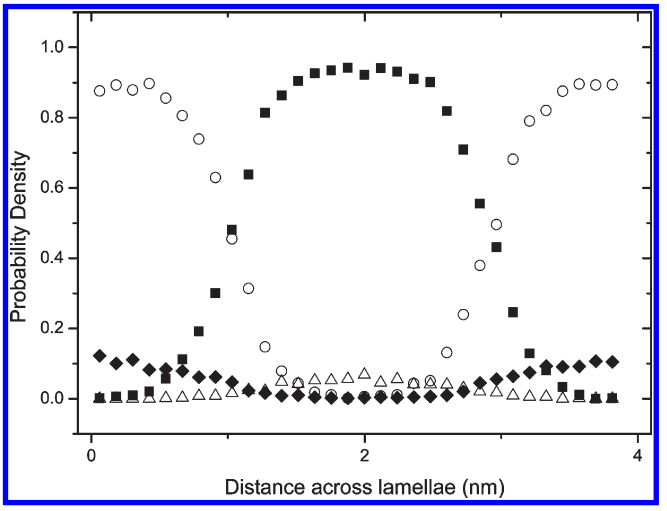

Figure 8. Typical probability density function across the lamellar phase showing tail, head, water, and oil beads. The graph shown is of 0.04 hexane mole fraction, $X_{sw} = 0.75$ (■) tail, (○) head, (◆) water, and (△) oil beads.

For hexane, the fwhm narrows with increasing hexane concentration. At low hexane concentration, it penetrates between the surfactant alkyl chains. However, as the hexane concentration increases, it starts to accumulate at the center of the bilayer, and behaves more like a penetrating oil. For both dodecane and octadecane, the fwhm broadens with increasing oil, which is consistent with the oil expanding the region in the middle of the bilayer. The fwhm's for the surfactant tail beads all increase with added oil, demonstrating an expansion of the bilayer width. However, this increase is smallest for hexane which is consistent with a more penetrating character.

Tail Conformations. The examination of bead probability density functions can be taken a stage further by looking at the distribution of each of the beads along the surfactant alkyl chain. These are labeled 1−4, where bead 1 is the bead that includes the terminal CH_3 group, situated in the center of the bilayer, and bead 4 is closest to the interface region. Figure 11 is an example of these bead density functions, showing the probability density for each individual tail bead across a single lamellar bilayer.

The probability density functions for beads 1 and 2 are single Gaussian peaks, while beads 3 and 4 are resolved into two separated peaks. The distance between a bead on one tail and the same bead on the other side of the bilayer is related to the breadth of the single peaks or the separation between twin peaks. For beads 1 and 2, the fwhm was measured, but for beads 3 and 4, which were considered as two separate peaks, the separation of the peaks was measured. The fwhm for bead 2 is generally about 5% broader than bead 1, suggesting a broader distribution of beads in position 2 than beads in position 1 across the center of the bilayer and indicating folding or interdigitation of the chains. For each oil, the fwhm increases with increasing oil concentration, although the rate of increase is larger for more swelling oils. As might be expected, the peak separation for beads at position 4 is greater than that of beads at position 3 by about 75% for all oils. Again, the peak separation increases with oil addition but is more pronounced in swelling than penetrating oils.

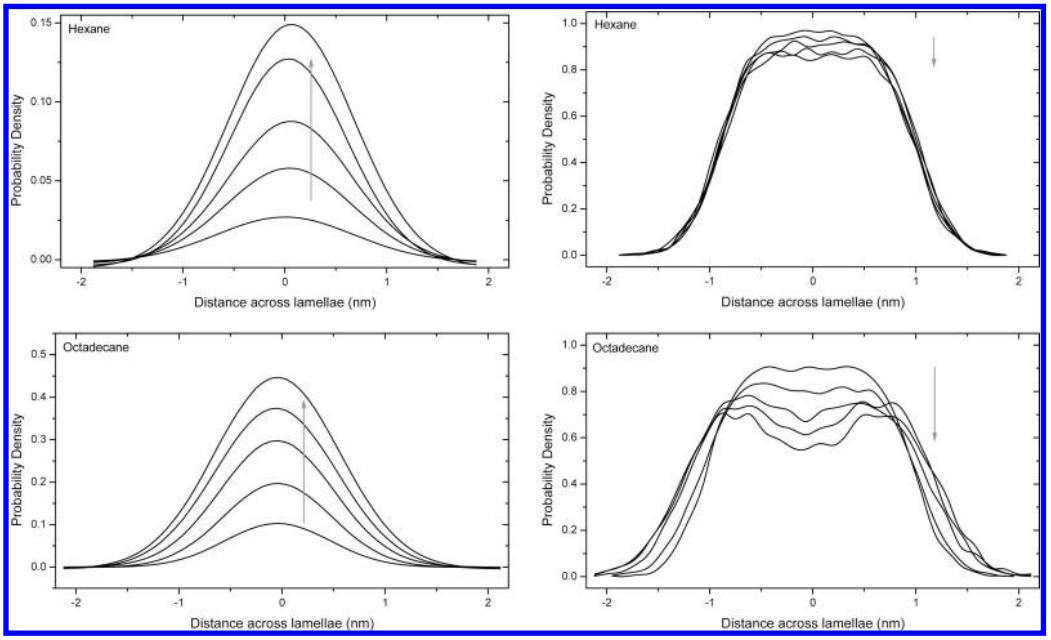

Figure 9. Probability density functions for oil (left) and tail (right) beads for hexane (top) and octadecane (bottom). Arrows indicate increasing oil concentration.

dx.doi.org/10.1021/jp108980p |J. Phys. Chem. B 2011, 115, 1385–1393

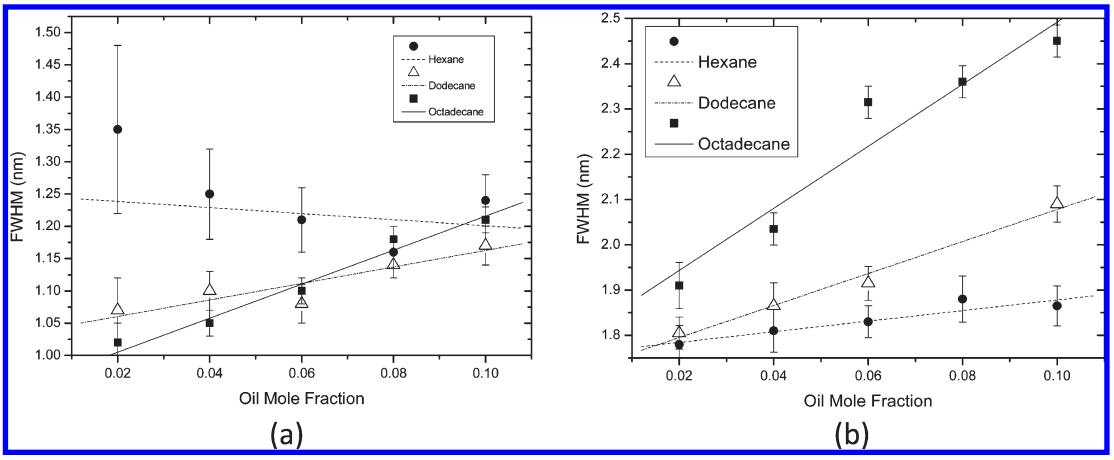

Figure 10. (a) The oil fwhm for increasing oil mole fraction. (b) The tail fwhm for increasing oil mole fraction. Lines are least-squares fits.

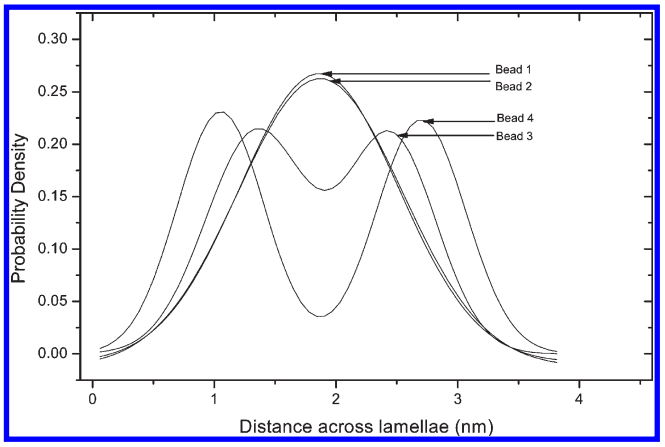

Figure 11. Alkyl tail bead probability density function example.

4. CONCLUSIONS

We have shown that using a DPD model it is possible to simulate the wide range of phase structures available in the binary surfactant−water experimental system and that these are attainable with physically realistic parameters.

With the addition of a ternary component, in this case oils, the DPD model reproduces to a large extent the experimental results.[3] Experimentally, oils destabilized phases with nonzero surface curvature, and the longer the oil, the more pronounced the effect. The simulation results also exhibit this for hexane and dodecane, where the phase transitions occur at lower mole fractions of dodecane than for hexane.

By studying the probability density function across the lamellar phase for the ternary systems, it was found that the terminal tail beads of the surfactant (the end of the tail) had a higher separation (measured by fwhm) than the penultimate tail beads for low concentrations of added oil and for all concentrations of added hexane. This may indicate some overlapping of the tails in the lamellar phase either by conformational folding or by interdigitation.

■ ACKNOWLEDGMENT

All simulations were performed using the SGI Altix 3700 supercomputer at the University of Central Lancashire's High Performance Computing Facility. In this work, the coarse grained molecular dynamics program COGNAC v5 part of OCTA[39] was used to perform all of the simulations. Input and output files were created and modified with Gourmet, the graphical user interface for OCTA. N.D. would like to thank the University of Central Lancashire for a studentship. We would also like to thank Guo Xiaohu, Sarah Dennison, and Marco Pinna for helpful discussions.

■ REFERENCES

(1) Baciu, M.; Holmes, M. C.; Leaver, M. S. *J. Phys. Chem. B* **2007**, *111* (4), 909.
(2) Baciu, M.; Olsson, U.; Leaver, M. S.; Holmes, M. C. *J. Phys. Chem. B* **2006**, *110* (16), 8184.
(3) Wang, Y.; Holmes, M. C.; Leaver, M. S.; Fogden, A. *Langmuir* **2006**, *22* (26), 10951.
(4) Ninham, B. W.; Chen, S. J.; Evans, D. F. *J. Phys. Chem.* **1984**, *88* (24), 5855.
(5) Holmes, M. C.; Leaver, M. S. Intermediate Phases. In *Bicontinuous Liquid Crystals*; Lynch, M. L., Spicer, P. T., Eds.; CRC Press, Taylor & Francis Group: Boca Raton, FL, 2005; pp 15−39.
(6) Hamley, I. W.; Castelletto, V.; Mykhaylyk, O. O.; Yang, Z.; May, R. P.; Lyakhova, K. S.; Sevink, G. J. A.; Zvelindovsky, A. V. *Langmuir* **2004**, *20* (25), 10785.
(7) Ekwall, P.; Mandell, L.; Fontell, K. *J. Colloid Interface Sci.* **1969**, *31*, 508.
(8) Holmes, M. C. *Curr. Opin. Colloid Interface Sci.* **1998**, *3*, 485.
(9) Leaver, M. S.; Fogden, A.; Holmes, M. C.; Fairhurst, C. E. *Langmuir* **2001**, *17* (1), 35.
(10) Oradd, G.; Gustafsson, J.; Almgren, M. *Langmuir* **2001**, *17* (11), 3227.
(11) Puntambekar, S.; Holmes, M. C.; Leaver, M. S. *Liq. Cryst.* **2000**, *27* (6), 743.
(12) Kunieda, H.; Ozawa, K.; Huang, K. L. *J. Phys. Chem. B* **1998**, *102*, 831.
(13) Kunieda, H.; Taoka, H.; Iwanaga, T.; Harashima, A. *Langmuir* **1998**, *14*, 5113.
(14) Kunieda, H.; Shinoda, K. *J. Dispersion Sci. Technol.* **1982**, *3* (3), 233.
(15) Fairhurst, C. E.; Holmes, M. C.; Leaver, M. S. *Langmuir* **1997**, *13*, 4964.
(16) Hoogerbrugge, P. J.; Koelman, J. M. V. A. *Int. Rev. Phys. Chem.* **1992**, *19* (3), 155.
(17) Moeendarbary, E.; Ng, T. Y.; Zangeneh, M. *Int. J. Appl. Mech.* **2009**, *1* (4), 737.
(18) Liu, H.; Qian, H. J.; Zhao, Y.; Lu, Z. Y. *J. Chem. Phys.* **2007**, *127* (14), 144903–1.
(19) Groot, R. D.; Rabone, K. L. *Biophys. J.* **2001**, *81* (2), 725.

(20) Ryjkina, E.; Kuhn, H.; Rehage, H.; Muller, F.; Peggau, J. *Angew. Chem., Int. Ed.* **2002**, *41* (6), 983.
(21) Yuan, S. L.; Cai, Z. T.; Xu, G. Y. *Acta Chim. Sin.* **2002**, *60* (2), 241.
(22) Schulz, S. G.; Frieske, U.; Kuhn, H.; Schmid, G.; Muller, F.; Mund, C.; Venzmer, J. *Tenside, Surfactants, Deterg.* **2004**, *41* (5), 230.
(23) Nakamura, H.; Tamura, Y. *Comput. Phys. Commun.* **2005**, *169* (1−3), 139.
(24) Huang, C. I.; Chiou, Y. J.; Lan, Y. K. *Polymer* **2007**, *48* (3), 877.
(25) Schulz, S. G.; Kuhn, H.; Schmid, G.; Mund, C.; Venzmer, J. *Colloid Polym. Sci.* **2004**, *283* (3), 284.
(26) Kranenburg, M.; Smit, B. *J. Phys. Chem. B* **2005**, *109* (14), 6553.
(27) Lyubartsev, A. P. *Eur. Biophys. J. Biophys. Lett.* **2005**, *35* (1), 53.
(28) Kranenburg, M.; Venturoli, M.; Smit, B. *J. Phys. Chem. B* **2003**, *107* (41), 11491.
(29) Groot, R. D.; Madden, T. J. *Struct. Dyn. Mater. Mesosc. Domain* **1999**, 288.
(30) Espanol, P.; Warren, P. *Europhys. Lett.* **1995**, *30* (4), 191.
(31) Groot, R. D.; Stoyanov, S. D. *Phys. Rev. E* **2008**, *78*, 5.
(32) Groot, R. D.; Warren, P. B. *J. Chem. Phys.* **1997**, *107* (11), 4423.
(33) Khasanshin, T. S.; Shchamialiou, A. P.; Poddubskij, O. G. *Int. J. Thermophys.* **2003**, *24* (5), 1277.
(34) *Research Chemicals, Metals and Materials*; Alfa Aesar: Ward Hill, MA, 2008.
(35) Clunie, J. S.; Goodman, J. F.; Symons, P. C. *J. Chem. Soc., Faraday Trans.* **1969**, *65*, 287.
(36) Le, T. D.; Olsson, U.; Mortensen, K.; Zipfel, J.; Richtering, W. *Langmuir* **2001**, *17* (4), 999.
(37) Hoffmann, H.; Ulbricht, W. *Tenside, Surfactants, Deterg.* **1998**, *35*, 421.
(38) Rendall, K.; Tiddy, G. J. T. *J. Chem. Soc., Faraday Trans. 1* **1984**, *80*, 3339.
(39) OCTA. 23-2-2010. www.octa.jp. 28-5-2010.